The invertebrate myosin filament: subfilament arrangement of the solid filaments of insect flight muscles

Gernot Beinbrech,* Francis T. Ashton,‡ and Frank A. Pepe‡

*Zoologisches Institut, Universität Münster, D-4400 Münster, Federal Republic of Germany; and ‡Department of Anatomy, School of Medicine, University of Pennsylvania, Philadelphia, Pennsylvania, 19104-6058 USA

ABSTRACT Transverse sections (~140 nm thick) of solid myosin filaments of the flight muscles of the fleshfly, *Phormia terrae-novae,* the honey bee, *Apis mellifica,* and the waterbug, *Lethocerus uhleri,* were photographed in a JEM model 200A electron microscope at 200 kV. The images were digitized and computer processed by rotational filtering. In each of these filaments it was found that the symmetry of the core and the wall was not the same. The power spectra of the images showed sixfold symmetry for the wall and threefold symmetry for the core of the filaments. The images of the filaments in each muscle were superimposed according to the sixfold center of the wall. These averaged images for all three muscles showed six pairs of subunits in the wall similar to those found in the wall of tubular filaments. From serial sections of the fleshfly filaments, we conclude that the subunits in the wall of the filaments represent subfilaments essentially parallel to the long axis of the filament. In each muscle there are additional subunits in the core, closely related to the subunits in the wall. Evaluation of serial sections through fleshfly filaments suggests that the relationship of the three subunits observed in the core to those in the wall varies along the length of the filaments. In waterbug filaments there are three dense and three less dense subunits for a total of six all closely related to the wall. Bee filaments have three subunits related to the wall and three subunits located eccentrically in the core of the filaments. The presence of core subunits can be related to the paramyosin content of the filaments.

INTRODUCTION

The contractile proteins of muscles are localized in thin and thick filaments. The length and diameter of the myosin containing thick filaments may be different depending on their content of myosin and of paramyosin, a protein filling the core of the filaments of many invertebrate muscles (Winkelman, 1976). The 18–20-nm diameter of the thick filaments of insect flight muscles is essentially constant regardless of differences in their paramyosin content, which may vary between 2% and 18% of the filament mass (Aust et al., 1980; Beinbrech et al., 1985). Cross sections of filaments with little paramyosin (~2% of the filament mass) appear tubular in electron micrographs. Those with a larger paramyosin content (≥9% of the filament mass) appear solid (Beinbrech et al., 1985). The function of paramyosin in muscle is not yet clear. Two possibilities have been suggested: (*a*) a mechanical role in providing added structural stability during tension development (Winkelman, 1976) and (*b*) an influence on the ATPase activity of the contractile proteins (Szent-Gyorgyi et al., 1971; Nonomura, 1974; Breuer et al., 1982). In either case interactions of paramyosin with myosin molecules of the thick filaments have to be expected. It is not yet clear whether this interaction affects the arrangement of the myosin molecules in the backbone of the filaments.

The myofibrils of the flight muscles of the fleshflies such as *Phormia terrae-novae* are unique in containing tubular and solid myosin filaments within one sarcomere (Beinbrech et al., 1985). In an earlier study the arrangement of the myosin rods in the wall of the tubular filaments has been analyzed. A pattern of six pairs of substructural elements was described in the wall of the filaments (Beinbrech et al., 1988). These substructural elements behaved like parallel rods on tilting of the section and were therefore considered to be subfilaments parallel to the longitudinal axis of the filaments. The aim of this work is to relate the substructural organization of insect flight muscles to their paramyosin content and to obtain information about the structural relationship between the paramyosin and myosin in the filament backbone. The myosin filaments that will be used in this study include those of the fleshfly, *Phormia terrae-novae* (~9% paramyosin), the waterbug, *Lethocerus uhleri* (~11% paramyosin), and the honey bee, *Apis mellifica* (~18% paramyosin). By studying the structural organization of these filaments with varying paramyosin content and comparing them with the structure of previously studied tubular filaments with very low paramyosin content (Ashton et al., 1987; Beinbrech et al., 1988), we can gain insight into (*a*) distinguishing the myosin-containing and paramyosin-containing structures and (*b*) the relationship between paramyosin content and the structure of the core of the myosin filament.

0006-3495/92/06/1495/18 $2.00

MATERIALS AND METHODS

The dorsolongitudinal flight muscles of the fleshfly, *Phormia terraenovae,* the waterbug, *Lethocerus uhleri* (gift of Dr. Michael Ferenczi), and the honey bee, *Apis mellifica,* were used throughout this work. Thoraces were cut into halves and fixed by the multistage fixation procedure described by Ashton and Pepe (1981). After osmium fixation the tissue was dehydrated in alcohol and acetone and embedded in araldite. Serial transverse sections (~ 140 nm thick) were cut with a model MT-2 microtome (DuPont Sorvall, Newtown, CT). They were stained by immersion of the grid in 1% uranyl acetate in methanol for 2 h and then in 0.25% lead citrate in 25/75 (vol/vol) ethanol-water for 2–3 h. The transverse sections were examined at 200 kV in a JEM-200 electron microscope (Japan Electron Optics Laboratory Company, Tokyo, Japan) with a side-entry goniometer stage. When necessary, the sections were tilted slightly to align the longitudinal axis of the filaments parallel to the electron beam. Regions close to the Z-band or the M-band were not used for study. Micrographs were obtained at a magnification of 100,000 for the honeybee and the fleshfly, and 80,000 for the waterbug. Electron micrographs of transverse sections were digitized on model p-1000 Photoscan (Optronics Engineering, Goleta, CA) with pixel size of 50 × 50 μm on the electron micrograph, corresponding to 0.5 m × 0.5 nm on the specimen for the bee and the fleshfly and to 0.625 × 0.625 nm for the waterbug.

The images selected for study, in each case, came from a single area of an electron micrograph. Images which were clearly disrupted or elongated were not used. Using this criterion for the fleshfly, 67 images were selected from an area containing 78. For the waterbug all the images in an area of 155 were used and for the honeybee 61 images were used from an area of 76. Computer image processing of these images was carried out on a VAX 11/750 (Digital Equipment Corp., Marlboro, MA). Programs were written in FORTRAN and used conventional Fourier algorithms. Cross-correlation alignment and rotational filtering were used to process the images. For cross correlation alignment of images, the SPIDER package of software provided by Dr. Joachim Frank was used (Frank et al., 1981*a*). Alignment of the images was done with respect to a reference image taken from the group to be aligned. The reference was chosen for uniformity of density distribution and definition of substructure, but the process was carried out several times with different reference images and checked for consistency. Three cycles of alignment were used. In the first cycle cross correlation was used to rotationally align the autocorrelation functions of each image with the autocorrelation function of a reference image. In the second stage of the first cycle, cross correlation was used on the images themselves, each image being translationally and rotationally aligned with respect to the reference image. In the third stage of the first cycle the aligned images were averaged by superimposition to form the reference image for the second cycle of alignment. The second and third cycles of alignment used the images themselves and not the autocorrelation functions. In the second cycle of alignment, the averaged image formed by superimposition from the first cycle was used as the reference image against which all individual images were rotationally and translationally aligned by cross correlation. These were then superimposed to form the reference for the third cycle, which repeated the procedure of the second cycle against this new reference. The center of mass (of pixel density) of the average image obtained by superimposition after the third alignment cycle was used for rotational filtering of the image and the rotational power versus frequency was plotted to determine the symmetry of the average image. Rotational filtering was performed using the general Fourier-Bessel framework laid down by Crowther and Amos (1971). These programs were the same as those used in previous work (Stewart et al., 1981; Pepe et al., 1986). The input images were initially expressed in Cartesian coordinates and were transformed to polar coordinates by bilinear interpolation. Circumferential Fourier transforms were produced at a selected number of radial steps, generally one step per pixel, and a power spectrum was generated showing the frequency components of the image at each radius, as well as the totals over all radii. Individual images were also rotationally filtered. In this case centers were determined by finding the point in each image where n-fold Fourier power was the highest percentage of total (nonzero order) power. When images were reconstructed this was done using the n-fold harmonics, i.e., for threefold symmetry including frequencies of 3, 6, 9, 12, 15. Images were observed on an advanced electronics design color graphics terminal and photographed with a color graphics camera from Matrix Instruments (Orangeburg, NY).

To determine the resolution of the average images, the phase residual test (Frank et al., 1981*b*) was used. For this test the aligned images were separated into two groups. The phase residuals were calculated for a series of rings from the Fourier transforms of the images in the two groups. For each ring the phase residual was calculated first for one image from each group and then repeated each time another image was added to each group. For each ring in the Fourier transform, plots of the phase residual after each addition were made. The resolution was determined by allowing a maximum phase residual of 45° (Frank et al., 1981*b*; Van Heel, 1987).

RESULTS

General description of the structure of the myosin filaments

Transverse sections through sarcomeres of the longitudinal flight muscles of the fleshfly, the waterbug, and the honey bee are shown in Fig. 1, *a*, *b*, and *c*, respectively. The sections pass through portions of the filaments which do not include regions close to the M-band or to the end of the filaments. The myosin filaments of these muscles have diameters in the range of 18–20 nm. In the case of the fleshfly, there are both solid and tubular filaments in the same myofibril with the solid filaments occupying the center of the myofibril and the tubular filaments occupying the periphery (Beinbrech et al., 1985). In Fig. 1 *a*, the filaments are mostly from the center of the myofibril and therefore are solid, but some of the peripheral tubular filaments can be seen on the left side. The core of the tubular filaments is more or less free of electron-dense material. The solid filaments of the fleshfly on the other hand show a weak overall staining with more intensely stained elements (dots or elongated structures) corresponding to the walls and also in the core (in Fig. 1 *a*) with a small area of the center itself being mostly free of electron dense spots. Therefore, although we are referring to these as solid compared to tubular filaments, there is a small portion of the core which is free of dense spots. This same arrangement of densities was observed for all of the filaments of the longitudinal flight muscles of the water bug (*Lethocerus*) (Fig. 1 *b*). Sarcomeres of the flight

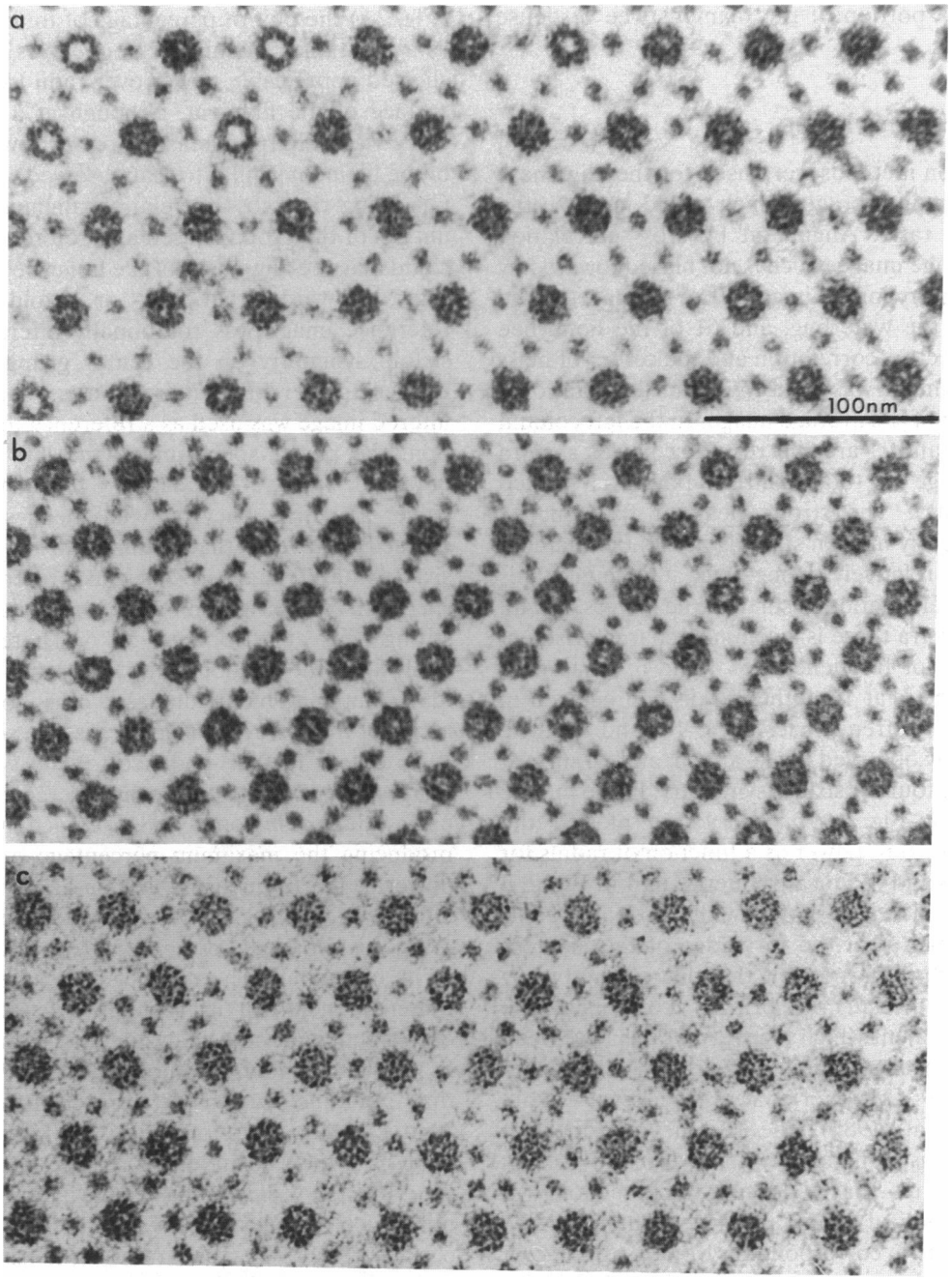

FIGURE 1 Transverse sections of the solid myosin filaments of insect flight muscles. (*a*) The fleshfly, *Phormia terrae-novae,* has both solid and tubular (on the left side) myosin filaments. Note the distribution of dense subunits and a weak overall density in the solid filaments. Although these filaments are essentially solid, note that there is a small core devoid of subunits. (*b*) In the waterbug, *Lethocerus uhleri,* all the myosin filaments look very similar to the essentially solid filaments of the fleshfly. (*c*) All of the myosin filaments of the honeybee, *Apis mellifica,* are solid. In this case the dense subunits are uniformly distributed in the transverse section. There is no indication of a small core devoid of subfilaments.

muscles of the honey bee also contain exclusively solid myosin filaments. In this case the substructural elements are distributed all over the cross sections of the filaments and there is no portion of the filament free of dense spots (Fig. 1 *c*).

Symmetry of the images

Cross-correlation methods were used for the alignment of images to obtain averages which would increase the signal to noise ratio. Alignment by cross correlation gives us an average image which is not biased toward any particular symmetry for the images. The 67 images of the fleshfly, 155 of the waterbug, and 61 of the honeybee were aligned by cross correlation and the center of mass of the average image was used to obtain the rotational power spectrum of the average image. In the left column of Fig. 2, *a*, *b*, and *c*, are the resulting power spectra where percentage of total nonzero power is plotted against frequency. The strong peak at frequency 1 results from slightly uneven staining across the filament profiles and the relatively strong peak at frequency 2 is related to slight elongation of some of the images. For all three power spectra there is a common characteristic of peaks of power for frequencies of 4 and 6. In a and c there is also a peak at 12. Other peaks can be seen in individual cases at frequencies of 8, 10, and 11. The more consistently observed peaks at 4, 6, and 12 suggest the possibility of four- or sixfold symmetry. In the middle two columns for Fig. 2, *a*, *b*, and *c* are plotted the percentage of nonzero power as a function of radius for frequencies of 4 and 6. For a frequency of 4 in Fig. 2, *a* and *b*, the bower increases sharply with increasing radius from 7.5 nm which is at the very edge of the filament (radius of 9–10 nm). It is possible that this symmetry may be related to the myosin cross-bridges projecting to the surface of the filament which in invertebrates have been reported to be arranged in a fourfold helical arrangement (Wray, 1979; Crowther et al., 1985; Stewart et al., 1985; Kensler et al., 1985). The axial helical repeat of cross budges in insect flight muscles is 116 nm (Reedy, 1968), which means that a 140-nm-thick section will include one full helical repeat and part of the next. The increment in density corresponding to part of the next axial repeat could be responsible for the fourfold increase in power at the edge of the filament (Fig. 2, *a* and *b*). In contrast to this, in obth Fig. 2, *a* and *b*, the percentage of nonzero power as a function of radius at a frequency of 6 is appreciable starting at a radius of 3–4 nm. The radius at which appreciable power begins is consistent with the absence of structural density in a small central core of the images. The presence of sixfold power throughout the rest of the filament suggests that the structural organization in average images obtained by cross-correlation alignment for the fleshfly (Fig. 2 *a*) and the waterbug (Fig. 2 *b*) most likely has predominantly sixfold symmetry. In the case of the honeybee (Fig. 2 *c*) the plot of percentage of total nonzero power as a function of radius for frequencies of 4 and 6 both showed appreciable power over radii from 2 nm to the surface of the filament, although at a frequency of 4 there was a sharp increase in power toward the surface of the filament similar to that observed in Fig. 2, *a* and *b*. On doing the cross-correlation alignment, one of the images of the group is used as a reference. To see if we could bias the alignment of the honeybee images used in Fig. 2 *c* toward either four- or sixfold symmetry, the reference image was rotationally filtered for four- or sixfold symmetry on the center giving the maximum nonzero power for that frequency. When the fourfold filtered image was used as a reference for cross correlation, the power spectrum on the left in Fig. 2 *d* was obtained. There is no peak at a frequency of 4 but the power at a frequency of 6 has been substantially increased relative to that obtained in Fig. 2 *c*. When the sixfold filtered image was used as a reference the power spectrum on the right in Fig. 2 *d* was obtained showing a strong peak at a frequency of 6. Therefore it is most likely that the predominant symmetry of the average image obtained by the unbiased cross-correlation alignment for the honeybee (Fig. 2 *c*) is also sixfold.

To obtain further evidence for the symmetry of the images, they were rotationally filtered for frequency n using values of n from 3 to 8. For each image the center producing the maximum percentage of total nonzero power at the frequency n and its harmonics was determined. In many cases the power spectrum obtained using this center did not have a peak at the frequency n or its harmonics. The number of images with peaks at the frequency n or its harmonics was determined for each frequency n. On analyzing the symmetry of the wall of tubular filaments (Beinbrech et al., 1988), we found that excluding spurious densities in the core prevented erratic results. Therefore in this work we separated our analysis of the wall and the core. For the fleshfly and the waterbug the wall was analyzed using radii from 3.5 to 9 nm, which includes the wall and a small portion of the core material. We used radii from 0.5 to 3.5 nm to analyze the core. This completely excluded the wall of the filament. For the honeybee filaments we also used radii of 0.5–3.5 nm for the core. The structure of the wall was analyzed in two sections; for the inner portion using radii of 3.0–6.5 nm and the outer portion using radii of 4–9 nm.

Transverse sections of 67 fleshfly filaments were studied in this way. The highest percentage of images, which on analysis of the wall had peaks in the power spectrum at the frequency n for which the center was

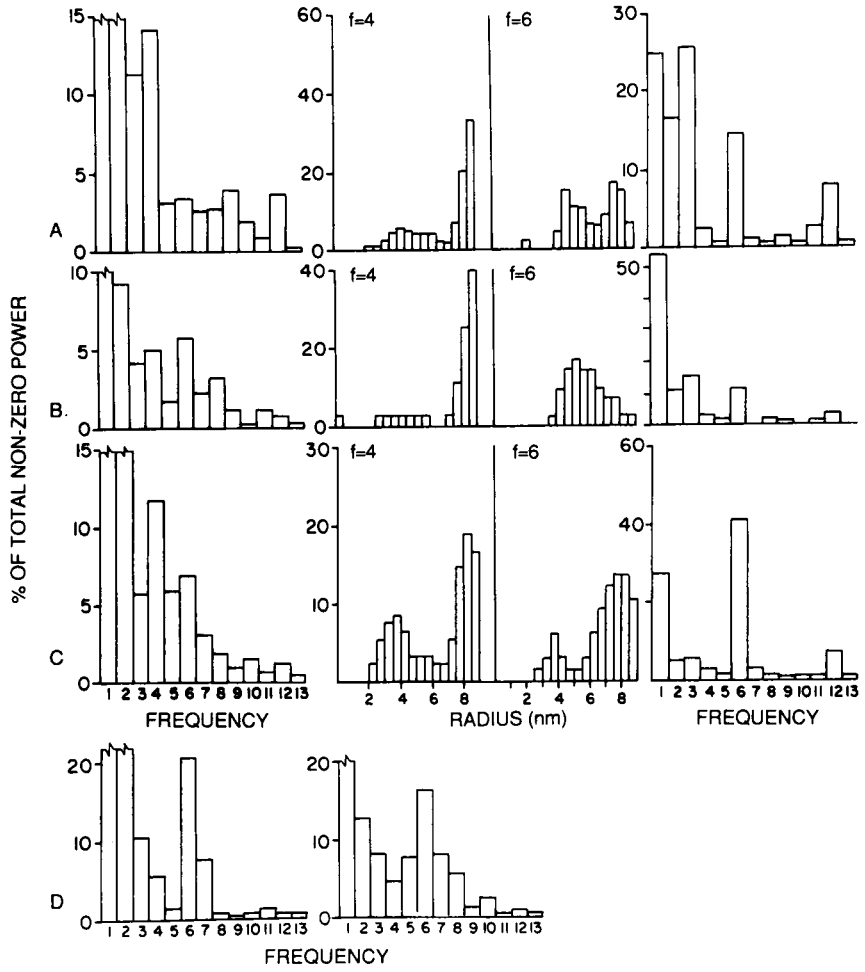

FIGURE 2 Power spectra of average images obtained by cross-correlation alignment of individual images. Average images were obtained by cross-correlation alignment of individual filaments and the rotational power spectrum was obtained from the average image using the center of mass (pixel density) as the center. In this way bias in favor of any particular symmetry was avoided. This was done for the (*A*) fleshfly, the (*B*) waterbug, and the (*C*) honeybee. In the first column for *A*, *B*, and *C* is plotted percentage of total nonzero power as a function of frequency. In the second column is plotted percentage of total power at a frequency of 4 as a function of radius. In the third column this is plotted for a frequency of 6. In the fourth column is percentage of total nonzero power as a function of frequency for the average of the same images aligned on their sixfold centers (see text) for comparison. (*D*, *left*) Percentage of total nonzero power as a function of frequency for the images of the honeybee used in *C*. In this case the cross-correlation analysis was done after filtering the reference image for fourfold symmetry to bias the alignment toward fourfold symmetry. (*D*, *right*) In this case the cross-correlation analysis was done after filtering the reference image for sixfold symmetry to bias the alignment toward sixfold symmetry. Cross-correlation alignment and averaging (first column of *A*, *B*, and *C*) results in peaks primarily at frequencies of 4 and 6. High power for frequency 1 results from slightly uneven staining across some of the filament images, and high power for frequency 2 is related to slight elongation of some of the images. From the radial density distributions (second and third columns), the power at a frequency of 4 appears to be related to the surface of the filament and may result from the cross-bridges protruding to the surface, whereas at a frequency of 6 it corresponds more closely to the filament backbone. An attempt to bias the alignment toward fourfold symmetry was not successful since the power at a frequency of 4 was not enhanced (*D*, *left*) while an attempt to bias the alignment toward sixfold symmetry was successful (*D*, *right*) leading to an enhancement of the power at a frequency of 6. The predominant symmetry in the images appears to be sixfold. Averages on the sixfold center of the individual images lead to enhancement of power at frequencies of 6 and 12 as would be expected for images with sixfold symmetry (fourth column of *A*, *B*, and *C*).

determined, occurred for a frequency of 6. In this case 59 (or 88%) of the images had peaks at a frequency of 6 or at both 12 and 18. For the waterbug, transverse sections of 155 filaments were studied in this way and all of them had peaks in the power spectrum at a frequency of 6 when the centers for maximum sixfold nonzero power were used. For all other frequencies studied there were fewer filaments with peaks at that frequency. For both the fleshfly and the waterbug, analysis of the core (i.e., radii 0.5–3.5 nm) showed them to have threefold

symmetry by this approach. The center determined for the sixfold symmetry of the wall and the threefold symmetry of the core were the same in both the fleshfly and the waterbug. Based on this analysis and on the cross correlation analysis (Fig. 2) we are confident that there is sixfold symmetry in the wall and threefold symmetry in the core of the filaments of the fleshfly and the waterbug.

Analyzing the outer portion of the wall (4–9 nm) in the 61 images of bee filaments in the same way we found that the power spectra of the largest number (54% or 88%) of the images showed evidence for sixfold symmetry in the wall. In the power spectra of five filaments where the sixfold symmetry was absent there were peaks of power at either a frequency of 12 or 18, and in the two additional ones there were peaks of power at both 12 and 18. Upon analyzing the core there were 58 (or 95%) of the images showing threefold symmetry. The rotational centers for the sixfold symmetry of the wall and the threefold symmetry of the core coincided only in a few of the 54 filaments that had both threefold centers and sixfold walls. The centers differed by a translation of 1.9 ± 0.76 nm (54 measurements). This difference suggests that the subunits of the core of the honeybee filaments are located eccentrically compared to the subunits of the wall. On analyzing the inner portion of the wall (radii 3–6.5 nm) we found threefold symmetry. The centers of threefold symmetry for the inner portion of the wall were concentric with the sixfold centers of the outer portion of the wall. Henceforth we will consider the threefold inner portion of the wall as core material. As with the fleshfly and the waterbug, analysis by both cross-correlation alignment and rotational filtering suggests a sixfold symmetry for the wall and a threefold symmetry for the core including the inner portion of the wall of the honeybee.

Based on these findings we can conclude that it is valid to apply filtering techniques which will enhance the sixfold symmetry of the wall or the threefold symmetry of the core.

Rotational filtering and superimposition of the images

To enhance the signal to noise ratio of the structure the images of the filaments were superimposed and averaged (Ashton et al., 1987; Beinbrech et al., 1988). In the case of the fleshfly and the waterbug where the centers for three- and sixfold symmetry coincide, the images were superimposed on the threefold center, which allows enhancement of both the three- and sixfold symmetrical elements when the images are rotated through the appropriate angles. The images were first rotated clockwise on the threefold center to bring the threefold elements into register. The rotational angle was then adjusted by the smallest angle necessary to enhance the sixfold structures in the wall. In the case of the honeybee where the threefold centers of three of the core elements and the sixfold centers of the outer portion of the wall did not coincide, average images were obtained on the different centers separately. An average image was produced by superimposing the individual images on the nonconcentric threefold centers of the core and these were superimposed again, using the sixfold centers of the outer portion of the wall. In all cases the images were first rotated on the threefold center by the smallest angles required to bring the threefold elements into register. For the fleshfly and the waterbug since the three- and sixfold centers coincide, the rotational alignment was then adjusted to maximize superimposition of both the sixfold structures in the wall and the threefold structures of the core. For the honeybee this adjustment was done after translation to the sixfold center of the wall. The power spectra obtained for the fleshfly, waterbug, and honeybee on these centers are shown in the last column on the right in Fig. 2, *A*, *B*, and *C*. In each case frequencies of 6 and 12 are enhanced. In the case of the fleshfly and the waterbug (Fig. 2, *A* and *B*) where the three- and sixfold centers coincide there is also an enhancement at a frequency of 3. In the case of the honeybee where the three- and sixfold centers do not coincide there is no appreciable peak at a frequency of 3 for the average on the sixfold centers. Averaging on the threefold centers gives a strong peak at a frequency of 3 with a smaller peak at a frequency of 6 (not shown).

Since each individual image in an area of the micrograph was rotated in the same way for alignment for superimposition, a plot of the frequency distribution of the angles of rotation should reveal if there are preferential orientations for the individual filaments in the lattice. The frequency distribution of the threefold angles as well as the total angles required for superimposition of the images did not show any preferential orientations. Since these muscles were fixed live, the state of the muscle is difficult to define. Whether or not this is a factor influencing the rotational orientation of individual filaments in the lattice is not known.

Fleshfly filaments

The average of 59 superimposed fleshfly images is shown in Fig. 3 *a*. In order to preserve the relationship between the threefold core and the sixfold wall the average image was rotationally filtered for threefold symmetry, and this is shown in Fig. 3 *b*. The corresponding filtered and unfiltered average images are closely similar. There are six pairs of densities in the wall of the filament and three core densities closely adhering to the inside wall of the

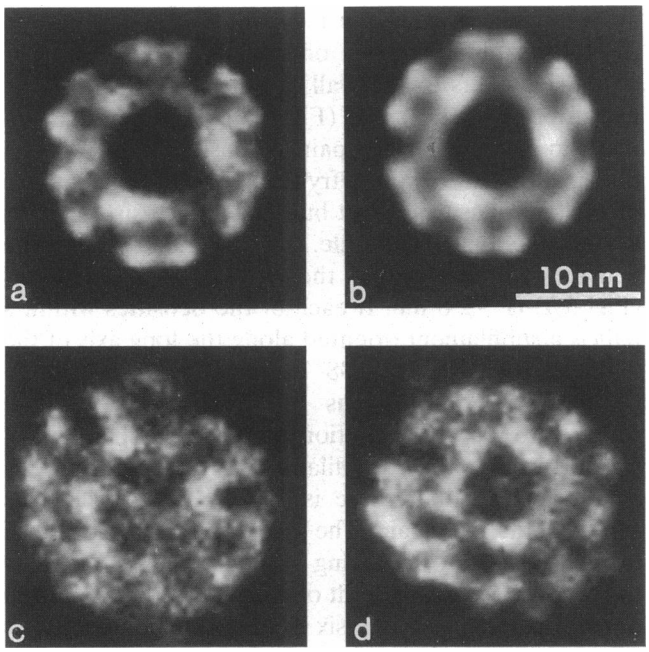

FIGURE 3 Subfilament organization in the myosin filaments of the flight muscles of the fleshfly, *Phormia terrae-novae*. These are negative images; i.e., high protein density is white. (*a*) Average of 59 individual images superimposed on the sixfold center of the wall. The sixfold center of the wall and the threefold center of the core coincided in these images. (*b*) The average image in *a* filtered for threefold symmetry. The wall structure is made up of six pairs of densities and the core has three densities apposed to the inner surface of the wall. These core densities are aligned between pairs of densities in the wall. The spacing between the elements of a pair is 2.8 nm and that between adjacent elements of neighboring pairs is 4.2 nm. Representative examples of individual filament images are shown in *c* and *d*.

filament. The core densities are positioned approximately between two pairs of densities in the wall. Representative examples of unfiltered individual images are shown in Fig. 3, *c* and *d*. In Fig. 3 *c*, two of the core elements are evident, a third appears displaced. In Fig. 3 *d*, most of the 12 subfilaments in the wall can be seen.

One question of concern was whether the position of the three core densities relative to the wall densities in Fig. 3, *a* and *b*, was the same along the length of the filaments. To check this three serial sections of the same filaments were studied. The same 42 filaments in an area were identified in three successive serial sections. The thickness of the sections was 140 nm so this represents a total of 420 nm along the length of each filament. All 42 filaments had sixfold symmetry in each of the three serial sections. The filaments in each section were superimposed and averaged as described above. The average image for each section was then filtered for threefold symmetry to observe the relation between the core densities and the wall. In Fig. 4 *a* are the unfiltered (left side) and filtered (right side) average images obtained from one section. In this case the core densities are pairs of densities in the wall, as is the case in Fig. 3, *a* and *b*. In Fig. 4 *b*, are the corresponding images for the same 42 filaments in the neighboring section. In Fig. 4 *b*, the three core densities are each related to a pair of densities in the wall instead of being positioned relative

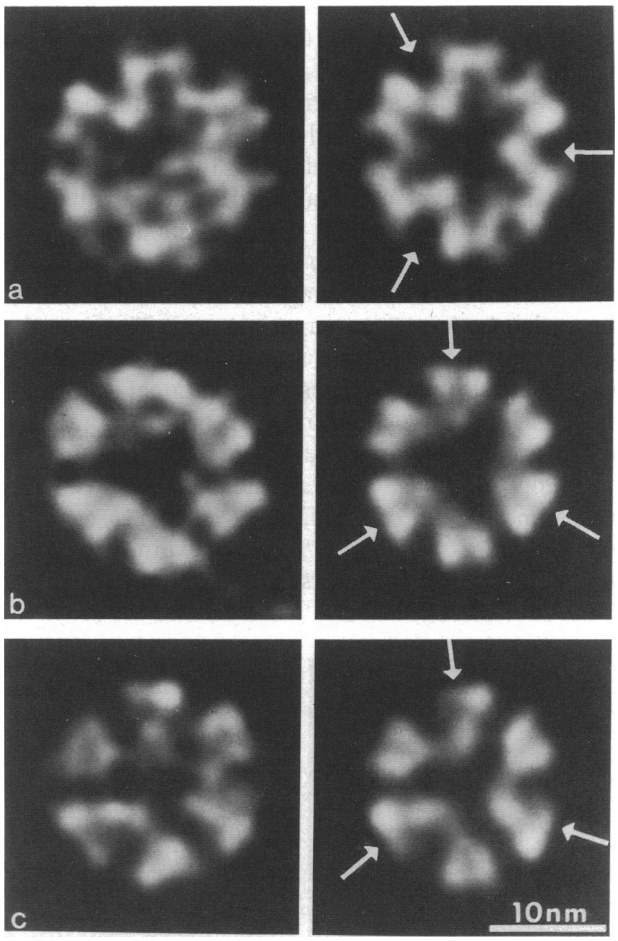

FIGURE 4 Relation between subfilaments of the core and the wall in the fleshfly, *Phormia terrae-novae*. This average image of the same 42 filament images in three serial sections is shown in *a*, *b*, and *c*. In each case the unfiltered average is on the left, and the corresponding threefold filtered image is on the right. These are negative images; i.e., high protein density is white. (*a*) The core subfilaments apposed to the inner wall of the filament are positioned between pairs of subfilaments in the wall. The position of the three core subfilaments is indicated by arrows in the filtered image. Section thickness is 140 nm. (*b*) In the neighboring section (thickness 140 nm) the core subfilaments are positioned in line with pairs of subfilaments in the wall. (*c*) In the third serial section (thickness 140 nm), the core subfilaments are again positioned in line with pairs of subfilaments in the wall. The relative position of the core subfilaments with respect to wall subfilaments appears to be erratic except that they are always apposed to the inner surface of the wall.

to the space between pairs of densities as in Fig. 4 *a*. Therefore, over a distance of about 140 nm the position of the core densities relative to the wall has changed. For the next serial section the images of the 42 filaments are shown in Fig. 4 *c*. The position of the core densities relative to the wall has not changed appreciably in this case from that observed in Fig. 4 *b* or over a distance of 140 nm. Therefore there does not appear to be a constant relationship or a consistent change in relationship between the core and wall densities along the length of the filament in the myosin filaments of the fleshfly.

Another aspect of the structure of the filaments that was investigated was whether the densities in the wall behave as subfilaments and if these subfilaments in the wall of the filament are parallel to or tilted relative to the long axis of the filament. To determine this, the 42 filaments used to obtain the data in Fig. 4 were used. For each filament the three images of the same filament in the serial sections were superimposed. This was done without rotation so that superimposition was made without consideration of possible rotational distortion of the filament from section to section over the total length of 420 nm covered by the three serial sections. The superimposed images for each filament were analyzed for symmetry. Out of the 42 images, 29 (i.e., 69%) had sixfold symmetry. These 29 images were averaged by superimposing the sixfold symmetrical structures. The average image is shown in Fig. 5 *a* and this was filtered for the sixfold symmetry of the wall (Fig. 5 *b*). The sixfold elements in the wall are clearly visible. In the unfiltered average image (Fig. 5 *a*), each element appears to be made up of a pair of densities. However, on filtering for sixfold symmetry (Fig. 5 *b*), the appearance of pairs of densities is lost but each of the six elements retains an elongated profile. The distance between the densities within a pair in the wall of fleshfly filaments (Fig. 3 *b*) is ~2.8 nm. If each of the densities within a pair is a subfilament oriented along the long axis of the filament, then a tilt of 0.38° over the length of 420 nm (i.e., three serial sections 140 nm thick) would be required to prevent resolution of the two subfilaments of a pair. In that pairs of subfilaments are observed in Fig. 5 *a*, it is likely that there is $<0.38°$ tilt between the subfilaments of a pair. The center to center distance between the units consisting of pairs of subfilaments in the wall is 6.8 nm, and a tilt of 0.9° would be required to obscure resolution of the six elements made up of pairs of subfilaments. Therefore the tilt of the subfilaments making up the wall of the filament is probably $<0.38°$ within a pair and $<0.9°$ for the units consisting of a pair, making them essentially parallel to the long axis of the filaments.

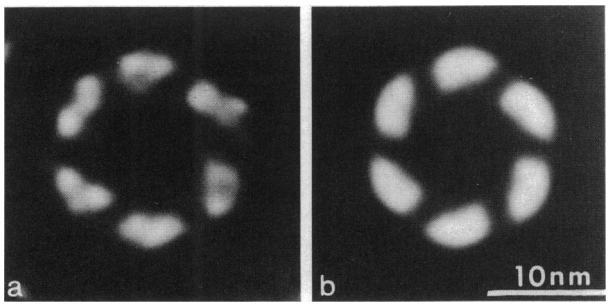

FIGURE 5 Evidence that the subfilaments in the wall of the myosin filaments of insect flight muscles of the fleshfly are parallel to the long axis of the filament. The three serial transverse images for each of the 42 filaments used in Fig. 4 were superimposed without rotation. This represents a total length of 420 nm along the filament. Of the 42 average images, 29 (i.e., 69%) had sixfold symmetry. These 29 were then averaged by superimposing the sixfold symmetrical structures. (*a*) The unfiltered average. Pairs of densities with spacings of about 2.8 nm are resolved in the average unfiltered image. Therefore, over a 420-nm length, the tilt between the subfilaments of a pair is $<0.38°$. (*b*) The sixfold filtered average. The six units representing the pairs of subfilaments spaced ~6.8 nm apart remain resolved in the average filtered image. Therefore, over a 420-nm length, the tilt between these units is $<0.9°$. Thus, the subfilaments in the wall of the filaments are essentially parallel to the long axis of the filament.

Rotational power as a function of radius for the images in Fig. 3, *a* and *b*, is shown in Fig. 6. This is shown for a frequency of 3 because of the threefold symmetry of the core and for frequencies of 6 and 12 because of the sixfold symmetry of the wall. At a frequency of 3 the maximum power occurs at a radius of 3.8 nm corresponding to the three subfilaments in the core of the filament. For frequencies of 6 and 12 the maximum power at radii of 7.5 and 8 nm respectively corresponds to the larger radius at which the subfilaments of the wall are located. This is summarized in Table I *B*.

Waterbug filaments

Observation of the individual filtered images led to the conclusion that almost all of the images could be separated into two groups. In both groups the densities in the wall were arranged in six pairs around the wall of the filament. There were also three strong and three weak densities apposed to the inner surface of the wall. In 74 of the images the three strong and three weak densities were positioned in relation to the gap between pairs of densities in the wall (Fig. 7 *a*), and in 53 images the densities were positioned relative to one of the two densities of a pair in the wall (Fig. 7 *b*). Eight of the images could not be fit into either of these groups because the positions of the core densities relative to the wall were somewhere in between. The additional 20 individual images had less clear structure in the wall although the wall had sixfold symmetry. From the two

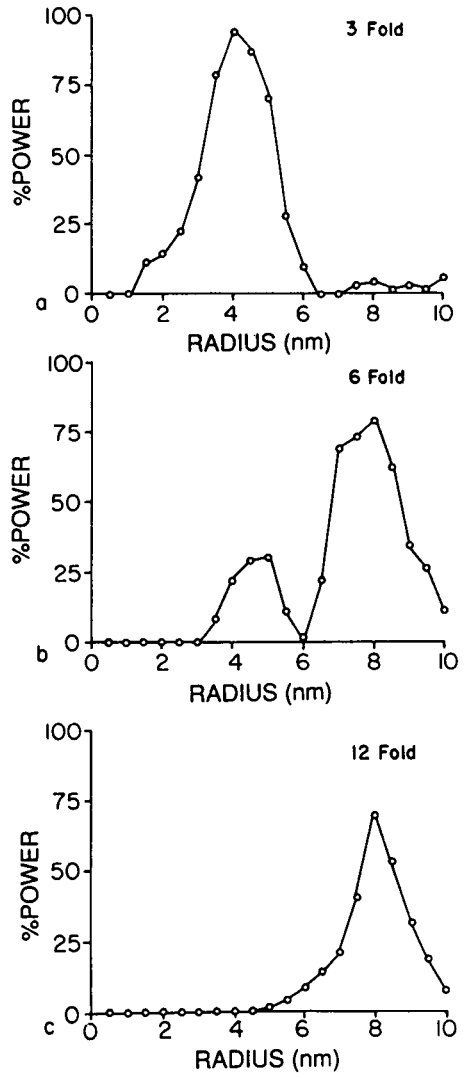

FIGURE 6 Plots of percent of total power as a function of radius for fleshfly myosin filaments. These are for the average of 59 individual images shown in Fig. 3, *a* and *b*. (*a*) At a frequency of 3, the maximum power occurs at a radius of 3.8 nm corresponding to the position of the three core subfilaments. (*b* and *c*) At frequencies of 6 and 12, the maximum power occurs at a larger radius (7.5 and 8.0 nm, respectively) corresponding to the position of the subfilaments in the wall.

groups of images (Fig. 7, *a* and *b*) there were nine images in which the six densities of the core were about equally strong and these showed sixfold symmetry in the core.

Power as a function of radius is plotted in Fig. 8 for frequencies of 3, 6, and 12 for the average of all the filaments. As was seen with the fleshfly, for the waterbug the peak for a frequency of 3 (Fig. 8 *a*) corresponds to the radius of 3.6 nm at which the core densities are present and the peaks for frequencies of 6 (Fig. 8 *b*) and 12 (Fig. 8 *c*) correspond to the radii at which the wall densities are present. This is summarized in Table I *B*.

Honeybee filaments

Because of the difference in the centers of symmetry for three of the six core elements and the wall the images of the individual filaments were superimposed in two ways: (*a*) using the rotational centers for maximum threefold symmetry of the eccentric core elements and (*b*) using the rotational centers for maximum sixfold symmetry of the outer portion of the wall. The average of the 54 filaments superimposed on the sixfold centers is shown in Fig. 9 *a*. The wall is composed of six pairs of densities. Some of these join at smaller radii to form V-shaped structures. Weaker densities with no apparent symmetry can be seen in the center of the average image. If this image is rotationally filtered for sixfold symmetry the differences in structure between the pairs of densities around the wall in the unfiltered average image (Fig. 9 *a*) is lost and six V-shaped structures are observed as in Fig. 9 *b*.

A group of filaments (36) with particularly strong power at a frequency of 3 in the core (radius 0.5 to 3.5 nm) were averaged separately on the sixfold center as described above. The average image is shown in Fig. 9 *d*, and it is very similar to that using all 54 filaments in Fig. 9 *a*. The V-shaped elements appear to be alternatively arranged with pairs of densities around the wall of the filament. There are also asymmetrically arranged units of differing density in the core. On filtering this image for sixfold symmetry an image similar to that in Fig. 9 *b* was obtained as shown in Fig. 9 *e*. This image does not correspond structurally to either the unfiltered average of 54 images (Fig. 9 *a*) or 36 images (Fig. 9 *d*). For that reason the image in Fig. 9 *d* was filtered for threefold symmetry instead of sixfold symmetry with the result shown in Fig. 9 *f*. As in the unfiltered average image, pairs of densities alternate with V-shaped structures in the wall. In the core, there are three weak densities which probably correspond to the asymmetrically placed threefold elements in the core.

Measurements were made on the densities observed in the wall of the threefold filtered image (Fig. 9 *f*). The center to center distance between the two elements of a pair of densities is 2.5 nm, the distance between the two arms of a V is 3.1 nm, and the distance between one of a pair of densities and the neighboring arm of a V is 4.4 nm. These distances are indicated in the diagrammatic representation in Fig. 13 *a* (q.v.).

As described above the images of the individual filaments were also superimposed using the centers for maximum threefold power of the eccentric core elements of the filaments. In the average unfiltered image (Fig. 9 *g*), three strong densities can be observed surrounded by some asymmetrically arranged material. This average image filtered for threefold symmetry is shown in Fig. 9 *h*. The lack of organized structure in the

TABLE I **Structural parameters of the backbone of the myosin filaments of insect flight muscles**

A. Paramyosin content (percentage by weight)

Solid filaments	
Fleshfly 9	(Beinbrech et al., 1985)
Waterbug 11	(Bullard et al., 1973; Levine et al., 1976)
Honeybee 18	(Aust et al., 1980)
Tubular filaments	
Fleshfly 2.7	(Beinbrech et al., 1985)
Housefly 2.7	(Beinbrech et al., 1985)

B. Radii (nm) at which 3-, 6-, and 12-fold symmetry is maximum

Solid filaments	3-fold	6-fold	12-fold
Fleshly	3.8	7.5	8.0
Waterbug	3.6	7.7	8.4
Honeybee	2.8	6.1	7.5
Tubular filaments			
Fleshly	—	5.5	7 (Beinbrech et al., 1988)
Housefly	—	6	9 (Beinbrech et al., 1988)

C. Center-to-center spacing (nm) of subfilaments in the wall

Solid filaments	Within a pair	Between adjacent subfilaments of neighboring pairs
Fleshly	2.8	4.2
Waterbug	3.6	4.8
Honeybee	2.5*	4.4
Tubular filaments		
Fleshfly	2.8	4.0 (Beinbrech et al., 1988)
Housefly	2.8	4.0 (Beinbrech et al., 1988)

*In this case there were alternating pairs of subfilaments and V-shaped elements in the wall (Fig. 9 *f*). The spacing within a pair of subfilaments is 2.5 nm and the spacing between the two arms of a V is 3.1 nm (Fig. 13 *a*). The average of these is 2.8 nm similar to the spacing in the fleshfly.

wall is consistent with an eccentric position of the three central elements compared to the wall of the filament. The center-to-center distance of the central elements is 4.5 nm.

Representative examples of unfiltered individual images are shown in Fig. 9, *c* and *i*. Structural elements corresponding to the sixfold structure of the wall and the eccentrically related threefold structure of the core are detectable in these individual images.

Plots of power as a function of radius are shown in Fig. 10. In Fig. 10, *a*, *b*, and *c*, respectively, are plots for frequencies of 3, 6, and 12 for the average image in Fig. 9 *d* in which the individual images were superimposed on the sixfold center of the wall. In Fig. 10 *d* is the plot for a frequency of 3 for the average image in Fig. 9 *g* in which the same individual images were superimposed on the eccentric threefold center of the core. The peak in Fig. 10 *a* at 2.8 nm corresponds in position to that in Fig. 10 *d* and represents the eccentric core densities. Because the threefold (Fig. 10 *d*) and sixfold centers (Fig. 10 *a*) do not coincide in the honeybee filaments, the corresponding peak in Fig. 10 *d* is much higher than that in Fig. 10 *a*. The peaks in Fig. 10, *b* and *c* at 6.1 and 7.5 nm, respectively, correspond to the position of the pointed end of the V-shaped elements (inner portion of the wall) alternating with the pairs of density (outer portion of the wall) in Fig. 9, *d* and *f*. This is summarized in Table I *B*.

Resolution

The phase residual test for resolution (Frank et al., 1981*b*; Van Heel, 1987) was applied to the images of the fleshfly used in this work. Using 58 of the 59 images of the fleshfly, these were split into two groups of 29 images. The phase residual is calculated between one image of each group and then for the cumulative average obtained by successively adding an image to each group. The averages were made on the threefold center rotationally aligned for superimposition of the structure of the threefold core and the sixfold wall (as in Fig. 3 *a*). The phase residual was calculated for each cumulative average for 12 Fourier rings corresponding to resolutions from 2.1 to 8.0 nm. The maximum acceptable phase residual of 45° (Frank et al., 1981*b*) was reached at a resolution of 2.9 nm (Fig. 11) with the averaging of 18 images in each of the two groups. This is a conservative method for determining resolution (Van Heel, 1987),

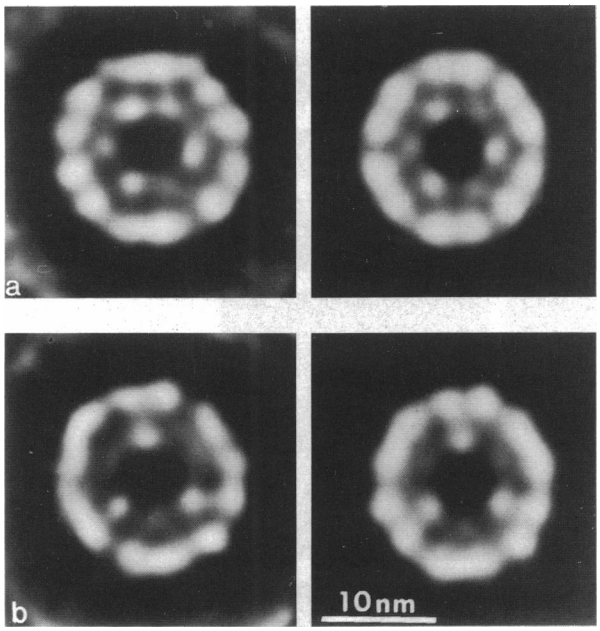

FIGURE 7 Subfilament organization in the myosin filaments of the flight muscles of the waterbug, *Lethocerus uhleri*. In these images, in general there were three dense and three less dense subfilaments apposed to the inner surface of the wall. The relationship between the core subfilaments and those in the wall fell into two major categories. The unfiltered average is on the left and the threefold filtered average is on the right. These are negative images, i.e., high protein density is white. (*a*) Average of 74 individual images in which the six core subfilaments are positioned between the pairs of subfilaments in the wall. (*b*) Average of 53 individual images in which the six core subfilaments are positioned in register with the pairs of subfilaments in the wall. As in *a*, the spacing between the subfilaments of a pair in the wall is 3.6 nm and that between adjacent subfilaments of neighboring pairs is 4.8 nm.

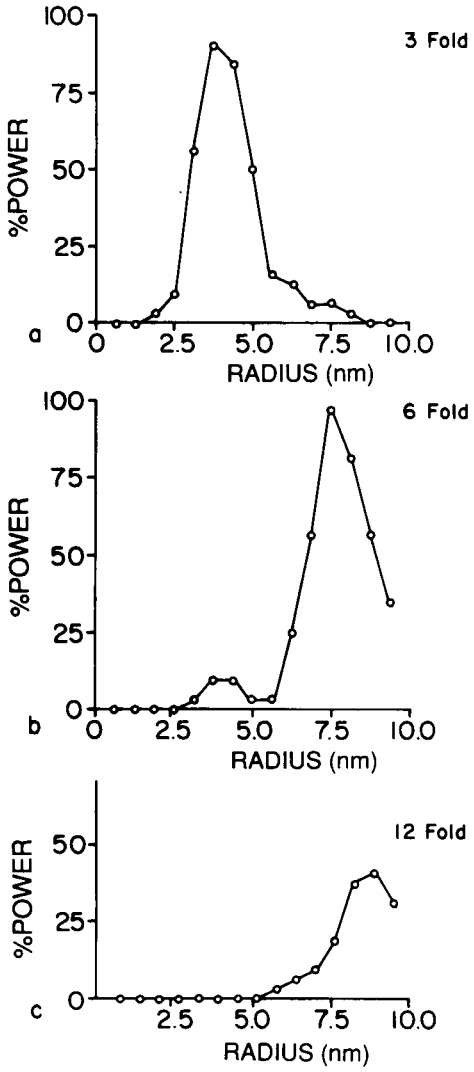

FIGURE 8 Plots of percent of total power as a function of radius for waterbug myosin filaments. These are for the average of all the images in Fig. 7, *a* and *b*. (*a*) At a frequency of 3, the maximum power occurs at a radius of 3.6 nm corresponding to the position of the core subfilaments. (*b* and *c*) At frequencies of 6 and 12 the maximum power occurs at a larger radius of 7.7 and 8.4 nm, respectively, corresponding to the position of the subfilaments in the wall.

and the result is consistent with the measured spacings of 2.8 nm between subfilaments within a pair (Table I *C*). All 58 of the images used had sixfold symmetry in the wall of the filaments. The phase residuals were also calculated using 154 of the 155 images of the waterbug and 60 of the 61 images of the honeybee and dividing these into paired sets of 77 and 30 images, respectively. For the waterbug where all the images had sixfold symmetry in the wall, the resolution obtained from the phase residuals was between 4.1 and 4.5 nm (Fig. 12 *b*). Because this is a conservative estimate, it is reasonably consistent with the measured spacings of 3.6 nm within a pair of subfilaments (Table I *C*). For the honeybee where only 54 of the 60 images used have sixfold symmetry in the wall, a conservative estimate of resolution of between 3.1 and 3.7 nm was obtained from the phase residuals (Fig. 12 *d*). This is also reasonably consistent with measured spacing of 2.5 nm between the subfilaments of a pair (Table I *C*).

Reproducibility

In the case of the fleshfly, the reproducibility of the images is verified by the observations of serial sections (Fig. 4). The same structure was observed for the wall in all three serial sections, and the three core subfilaments changed in position from the first to the second section. In Fig. 12 *a* are the final average images obtained with each set of images of the waterbug used to obtain the phase residuals in Fig. 12 *b*; and in Fig. 12 *c* are the final average images for each set of images of the honeybee

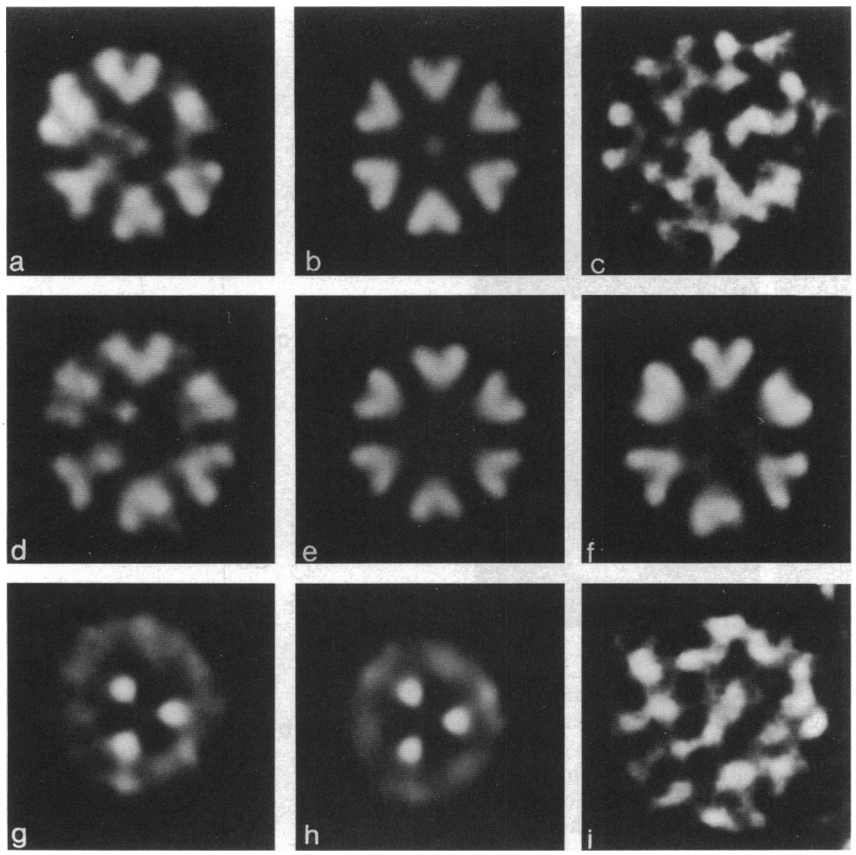

FIGURE 9 Subfilament organization in the myosin filaments of the flight muscles of the honeybee, *Apis mellifica*. Representative examples of individual filament images are shown in *c* and *i*. Note the uniform distribution of high protein densities throughout the filament in transverse section. These are negative images; i.e., high protein density is white. (*a*) Average of 54 individual images superimposed on the sixfold center of the wall of the filament (see text). The wall is composed of six pairs of densities, some of which are joined at smaller radii to form V-shaped structures. (*b*) The average image in *a* filtered for sixfold symmetry. There are six V-shaped structures around the circumference. (*c*) Representative example of an individual image. (*d*) Average of 36 of the 54 images in *a* chosen for their particularly strong power on the sixfold center of the core (see text). These were superimposed on the sixfold center of the wall as in *a* and an average image similar to that in *a* is obtained. (*e*) The average image in *d* filtered for sixfold symmetry. (*f*) The average image in *d* filtered for threefold symmetry on the sixfold center of the wall. The wall structure is made up of three pairs of densities alternating with three V-shaped structures corresponding closely to the average unfiltered image in *d*. There are also three weak densities in the core. (*g*) Average of the same images as in *d* only superimposed on the threefold center of the core. There are three dense units in the core and apparently structureless density in the wall. The three dense units in the core are located eccentrically with respect to the wall. (*h*) The image in *g* filtered for threefold symmetry. (*i*) Representative example of an individual image.

used to obtain the phase residuals in Fig. 12 *d*. The similarity of the paired images in Fig. 12, *a* and *c*, attests to the reproducibility of the images obtained for the waterbug and the honeybee.

DISCUSSION

There is considerable variation in the structure of invertebrate muscle myosin filaments (Baccetti, 1965, 1966; Gilev, 1966*a*, *b*; Halvarson and Afzelius, 1969; Reger, 1967; Reger and Cooper, 1967; Auber, 1967*a*, *b*; Hoyle, 1967; Hoyle and McNeil, 1968; Beinbrech et al., 1985). Although the myosin filaments of insect flight muscles all have approximately the same diameter of ~18–20 nm (Beinbrech et al., 1985) they can appear in cross section to be either tubular with a clearly visible, less dense core (Fig. 1 *a*, on the left side) or essentially solid with a much smaller, less dense, core (Fig. 1, *a* and *b*) or more completely solid (Fig. 1 *c*). In this study we have concentrated on insect flight muscles which have myosin filaments that appear solid or essentially solid in transverse sections in electron microscopy. These characteristically have a higher paramyosin content than the tubular filaments (Beinbrech et al., 1985). A major aim of this work is to observe the substructure of three

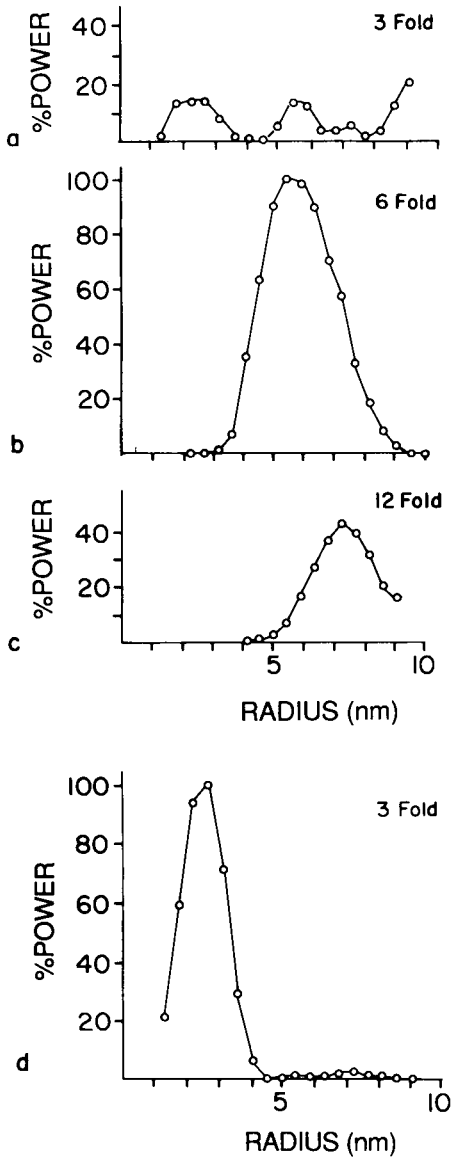

FIGURE 10 Plots of percent of total power as a function of radius for honeybee myosin filaments. (*a*, *b*, and *c*) Average of 37 images (Fig. 9 *d*) superimposed on the sixfold center of the wall. The radial distribution of power for frequencies of 3, 6, and 12 are shown in *a*, *b*, and *c*, respectively. (*a*) The peak between 1.5 and 3 nm corresponds to the three eccentric core subfilaments. (*b*) The peak at 6 nm corresponds to the alternating V-shaped structures and pairs of subfilaments around the periphery of the filament. The V-shaped structures probably result from the close apposition of three additional core subfilaments to three pairs of subfilaments in the wall (see text). (*c*) The peak at 7.5 nm corresponds to the arms of the V-shaped structures and the pairs of subfilaments. (*d*) The radial distribution of power for a frequency of 3 for the average image in Fig. 9 *g* in which the same images were superimposed on the threefold center of the core. The strong peak here at 2.8 nm represents the eccentric core densities and corresponds to the peak in *a* between 1.5 and 3 nm.

different insect flight muscle myosin filaments with varying paramyosin content and to compare this structure with (*a*) their paramyosin content and (*b*) the structure of the lower paramyosin content tubular filaments which have been studied previously (Beinbrech et al., 1988). From such comparisons we can identify the portion of the backbone structure that is related to the myosin component of the filaments and that which is related to the paramyosin content. In addition, using serial sections, we have been able to observe variability in the relationship between the paramyosin and myosin components along the length of the filament. We have also shown from serial sections that the wall of these filaments is made up of subfilaments arranged essentially parallel to the long axis of the filaments.

The approaches used in this work are analogous to those used in the single-particle averaging technique developed in the laboratory of Dr. Joachim Frank (Frank et al., 1988). In that work images are aligned by cross-correlation methods and then classified into groups by multivariate statistical analysis. Because of the noisy images available for this work, that approach could not be used directly. Instead two variations on this approach were made. In one case the images were first aligned by cross-correlation alignment, as done by Frank et al. (1988). This procedure is without bias with regard to symmetry. Evaluation of the average image obtained by this unbiased approach showed the presence of three- and sixfold symmetry. However, alignment of these relatively noisy images in this way was not precise enough to make the symmetrical structures clear enough to successfully classify different structures by multivariate statistical analysis. However, after having determined that the structures have three- or sixfold symmetry by the unbiased cross-correlation analysis, the structure present in the images could be enhanced by superimposing similar images on their three- or sixfold rotational centers and rotationally aligning them visually for maximum superimposition of the structural elements. Clearly different structural arrangements could be identified in individual images having the same symmetry. These were first classified into different groups visually and then averaged by superimposition. The different structural arrangements observed with varying paramyosin content (Figs. 3, 7, and 9) and in serial sections (Fig. 4, *a* and *b*) by using the same methods makes it unlikely that these results could be artifactually produced by the approach used.

Subunit structure of the wall

In all insect flight muscle myosin filaments studied so far, including those studied in this work and those with

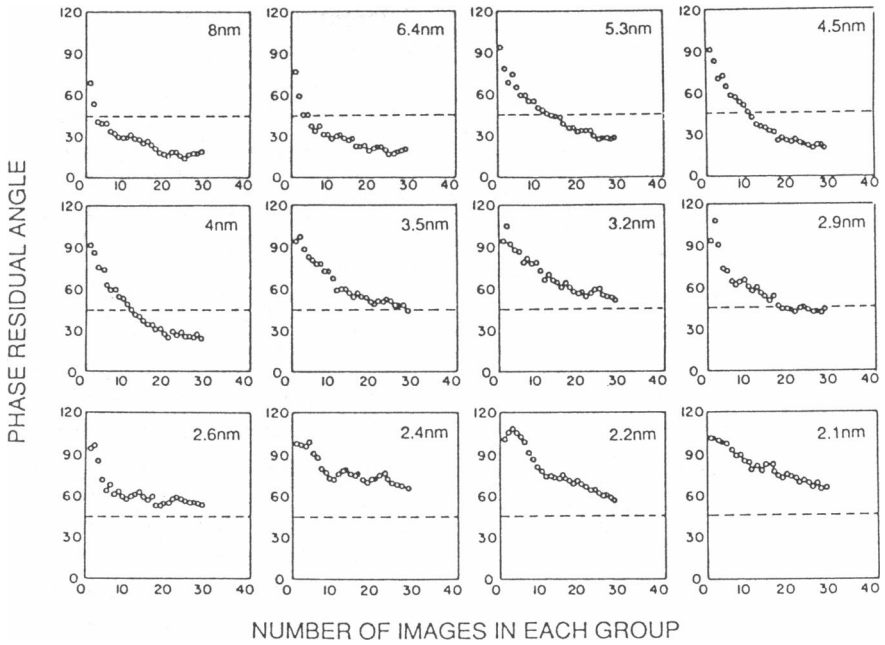

FIGURE 11 Phase residual test for resolution in fleshfly filament images. 29 pairs of images of fleshfly filaments aligned on their sixfold centers were used. The graphs show the phase residual angle calculated at the Fourier radius corresponding to the resolution indicated. Each data point represents the new phase residual after the addition of one image to each of the average images being compared. By using a maximum allowable phase residual of 45° (dashed lines), the average images have a resolution of 2.9 nm. All 58 of the images used had sixfold symmetry in the wall of the filaments. This is consistent with measured spacings of 2.8 nm between subfilaments within a pair (Table I *C*).

tubular backbones studied previously (Beinbrech et al., 1988), the structure of the wall of the filaments has been essentially the same. This same structure has also been observed for the wall of the fast abdominal muscles of the lobster (Ashton et al., 1987). The wall of all of these filaments consists of 12 subunits arranged in six pairs around the surface of the filament shown diagrammatically in Fig. 13 *b*. What may appear to be a variation on this structure (diagram in Fig. 13 *a*) was observed for the honeybee, in which alternating with three pairs of subunits there were three V-shaped elements with the point of the V directed inward toward the center of the filament (Fig. 9 *f*). However, because these filaments have an exceptionally high paramyosin content (Table I *A*), it is possible that paramyosin adhering to the inner wall of the filaments in close relation to three pairs of subunits in the wall could produce the observed V-shaped structure. This possibility will be discussed in more detail below.

The spacings measured between the subunits of a pair around the wall of the filament as well as between adjacent subunits of neighboring pairs are summarized for all of the insect flight muscle myosin filaments studied so far in Table I *C*. With the exception of the waterbug, the spacings are all closely similar with 2.5–2.8 nm between the subunits of a pair and 4.0–4.4 nm between adjacent subunits of neighboring pairs. In the case of the waterbug the spacings are larger, thereby being closer to those measured for lobster filaments (Ashton et al., 1987). The 3.6-nm spacing between the subfilaments of a pair compares with 3.4 nm in the lobster and the 4.8-nm spacing between adjacent subfilaments of neighboring pairs compares with 5.0 nm in the lobster. It is not clear what determines these spacings. There does not seem to be a relation to paramyosin content because the filaments of the waterbug (high paramyosin content) and the lobster (low paramyosin content) have essentially the same spacings in the wall; likewise for the honey bee and the fleshfly, which have very different paramyosin contents (Table I *A*) and very similar subunit spacings in the wall (Table I *C*). This suggests that differences in the myosin molecules themselves, which presumably make up the wall of the filament (see below), may be the major determinants of the packing of the subfilaments in the wall.

Relation between the structure in the wall and the core

From our observations of the constant wall structure, it is likely that the wall is the myosin-containing portion of the filament. There is a correlation of high paramyosin

content (9–18%) with solid filaments and low paramyosin content (2%) with tubular filaments (Table I *A*). Among the solid filaments there is also a correlation between the number of subfilaments in the core and paramyosin content. Considering that the V-shaped elements of the wall of the honeybee result from three core subfilaments apposed to the inner surface of the wall, then the honey bee filaments with 18% paramyosin have six subfilaments in the core (Fig. 9 *f*) and this is consistent with the presence of 3 subfilaments in the solid filaments of the fleshfly (Fig. 3 *b*) which have ~9% paramyosin. The waterbug has six core subfilaments, but in this case three of the six in most cases are of lower density (Fig. 7), consistent with a paramyosin content of 11% (Table I *A*), which is in between that of the honeybee and the fleshfly. Therefore there seems to be a direct correlation between the number of core subfilaments and paramyosin content.

Different structural relationships between the core and the wall were observed (Figs. 3 and 7), and the question arose as to whether these different relationships might be representative of different positions along the length of the filament. To answer this, serial sections of the myosin filaments in the fleshfly were studied and it was found that the position of the subunits in the core changes relative to the structure of the wall at different positions along the filament (Fig. 4). As has been previously observed in lobster muscle (Ashton et al., 1987), the change in position of the core material relative to the wall did not show a consistent pattern (compare Figs. 4, *a*, *b*, and *c*). In the case of lobster filaments where serial sections throughout the length of the filament were studied the core material changed in position erratically from section to section, in some cases not changing over long distances. Although serial sections were not studied for the waterbug, different relationships were also observed between the core and wall subunits (Figs. 7, *a* and *b*). In that the subfilaments of the wall have been shown by superimposition of serial sections to be essentially parallel to the long axis of the filament (Fig. 5), the change in relation between core and wall material must occur by shifting of the core material relative to the structure of the wall. We conclude that there is not a fixed or regularly changing

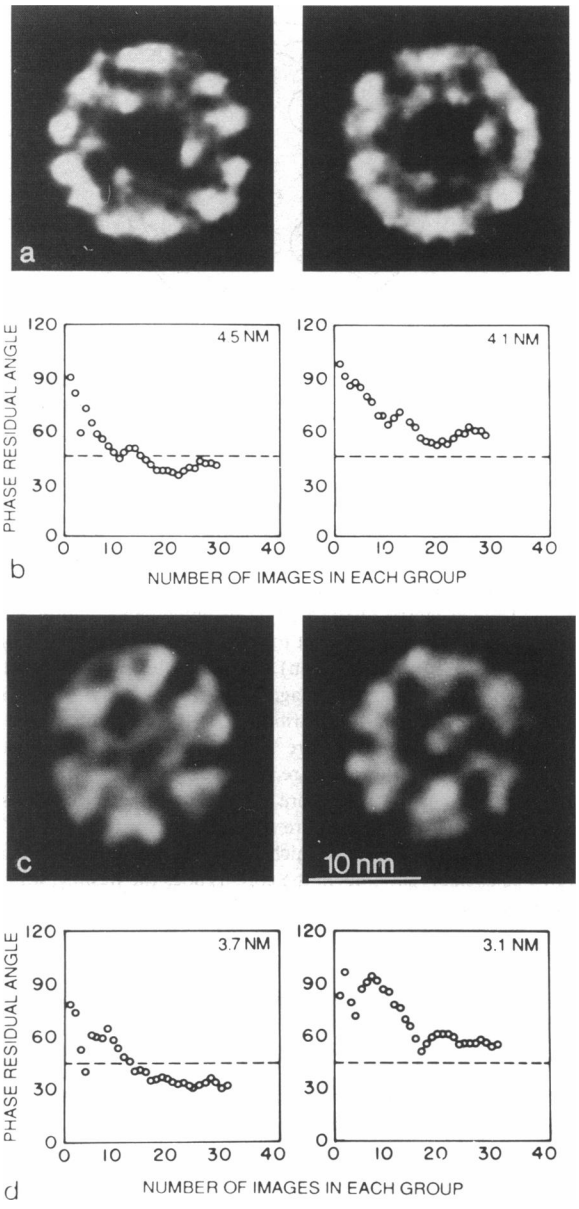

FIGURE 12 Phase residual test for resolution in waterbug and honeybee filament images. The phase residuals were obtained as in Fig. 11 for the fleshfly images and as described more fully in the text. (*a*) On the left is the final average of 77 of the images of a paired set for the waterbug and on the right the final average of the other 77 images used in determining the resolution using the phase residual test. These are negative images; i.e., high protein density is white. Note the similarity of the two images. (*b*) The graphs show the phase residual angle calculated at the Fourier radius corresponding to the resolution indicated, as in Fig. 11. By using the maximum allowable phase residual of 45° (dashed lines), the average images have a resolution of between 4.1 and 4.5 nm. All the images used had sixfold symmetry in the wall of the filaments. Because this is a conservative estimate of resolution, it is reasonably consistent with measured spacings of 3.6 nm between subfilaments within a pair (Table I *C*). (*c*) On the left is the final average of 30 of the images of a paired set for the honeybee and on the right the final average of the other 30 images. These are negative images; i.e., high protein density is white. Note the similarities of the two images. (*d*) The graphs show the phase residual angle calculated at the Fourier radius corresponding to the resolution indicated, as in Fig. 11. By using the maximum allowable phase residual of 45° (dashed lines), the average images have a resolution of between 3.1 and 3.7 nm. In that 54 of the 60 images had sixfold symmetry in the wall and in that this is a conservative estimate of resolution, it is reasonably consistent with measured spacings of 2.5 nm between the subfilaments of a pair (Table I *C*).

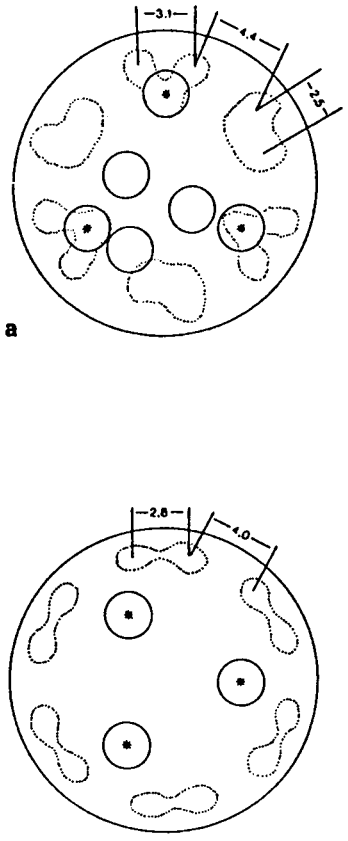

FIGURE 13 Diagrammatic representation of the relationship of core subfilaments and wall subfilaments in the honeybee (Fig. 9) and the fleshfly (Fig. 3). (*a*) The honeybee. The orientation of this diagram is the same as that of the average image in Fig. 9 *f*. The dashed tracings outline the density distribution of the elements in the wall. Three circles with asterisks indicate core elements that form the apices of the V-shaped elements. These elements have the same center of symmetry as the sixfold wall. The three additional circles (without asterisks) represent the eccentrically located core subfilaments whose center is displaced by 1.9 nm with respect to the sixfold center of the wall (see Fig. 9 *g* and text for discussion). (*b*) The fleshfly. This diagram corresponds to the average image in Fig. 3, *a* and *b*. The dashed tracings outline the density distribution of the elements in the wall. The threefold center of the core and the sixfold center of the wall coincide. Three core densities are indicated by circles with asterisks. These may correspond to the core elements marked with asterisks in the honeybee diagram. There are no additional core subunits in the fleshfly. Thus, the honeybee which has 18% paramyosin appears to have twice as many subunits in the core as does the fleshfly, which has 9% paramyosin.

structural relationship between the core material and the structure of the wall.

In the case of the honeybee the dominant threefold symmetry of the core material was not centered with respect to the sixfold symmetry of the wall, as was the case for the fleshfly and the waterbug. The honeybee also has much higher paramyosin content. In the wall of the honeybee, three pairs of subfilaments alternate with V-shaped elements (Fig. 9 *f*). These V-shaped elements could result from the close apposition of some of the core material to the wall in a pattern similar to that in Fig. 7 *b* for the waterbug or to that in Fig. 4, *b* and *c*, for the fleshfly. In this case part of the core material would have a similar relationship to the wall as in the fleshfly and the waterbug, i.e., concentric with the center of symmetry of the wall, and part would be eccentrically located with respect to the center of symmetry of the wall (Fig. 9, *g* and *h*). It is noteworthy that the eccentrically located core material also has threefold symmetry. A diagrammatic representation of the possible relationship between the core material and the wall in the honeybee is shown in Fig. 13 *a*.

Structural comparison between invertebrate and vertebrate myosin filaments

There are some similarities and some differences in the structural organization of invertebrate and vertebrate myosin filaments. For instance, the subfilaments in the wall of invertebrate myosin filaments have spacings varying from 3 to 5 nm (Table I *C*; Ashton et al., 1987), which are similar to the spacings between subfilaments in vertebrate skeletal muscles (Pepe et al., 1986). In addition there is evidence in this and previous work that in both invertebrate (Fig. 5; Ashton et al., 1987; Beinbrech et al., 1988) and vertebrate (Pepe and Dowben, 1977; Pepe et al., 1981) filaments, the subfilaments are essentially parallel to the long axis of the filament. The major structural differences between vertebrate and invertebrate myosin filaments consist of (*a*) the presence of paramyosin in the core of invertebrate filaments and the absence of core protein in vertebrate filaments, (*b*) the tubular arrangement of the myosin subfilaments in invertebrate filaments and the closely triangular and solid arrangement of vertebrate filaments, (*c*) the sixfold symmetry of the myosin-containing wall of invertebrates and the threefold symmetry of vertebrate filaments, and (*d*) the four-start helical arrangement of myosin cross-bridges on the surface of the invertebrate filaments (Wray, 1979; Crowther et al., 1985; Stewart et al., 1985; Kensler et al., 1985) consistent with the presence of 12 subfilaments; and the three-start helical arrangement of cross-bridges on the vertebrate filaments (Varrano-Marston et al., 1984; Kensler and Stewart, 1983; Ip and Heuser, 1983) consistent with the presence of nine subfilaments (Pepe et al., 1986). In addition to these differences vertebrate filaments are all ~1.6 μm in length whereas invertebrate filaments can vary considerably in length. In spite of these differences, the similarities in myosin subfilament spacings and the parallel

alignment of the myosin subfilaments suggests that there are some basic structural constraints on the organization of myosin molecules in widely varying types of filaments.

Invertebrate myosin filaments other than those of the insect flight muscles can be even more widely different from vertebrate myosin filaments. For instance, the myosin filaments of molluscan muscles have widely varying diameters and lengths within the same cell and have densely packed paramyosin cores (Bennett and Elliott, 1981). Probably the most complex myosin filaments studied so far are those of the body wall muscles of the nematode *Caenorhabditis elegans,* which contain two different myosins on the surface and a core consisting of an outer layer of paramyosin and an inner core structure related to the presence of several different proteins (Epstein et al., 1988). The basic similarities and differences in the organization of the myosin molecules in these very different myosin filaments remains to be determined.

A method which has been used to uncover structural units of organization in myosin filaments is to treat separated native filaments with reagents that will splay them into correspondingly smaller units. This has been done successfully with the myosin filaments of the flight muscle of the honeybee (Fan et al., 1966) and with native vertebrate skeletal myosin filaments (Maw and Rowe, 1980; Pepe, 1982). In the case of the honeybee flight muscle the filaments splayed into six units corresponding to the pairs of subfilaments in the wall, as described in this work, and a seventh unit corresponding to the core. In the case of vertebrate skeletal muscle the filaments splayed into three units, each of which would therefore correspond to three of the nine subfilaments observed in the backbone of the filament (Pepe et al., 1986). Splaying into these units suggests the presence of different interactions between the subfilaments within a unit and between units. For invertebrate muscles these different interactions relate to the sixfold symmetry of the wall and for vertebrate muscle to the threefold symmetry of the shaft of the filament.

This work was supported by U.S. Public Health Service grant HL-15835 to the Pennsylvania Muscle Institute, Basic Research Support Grants 2-S0-RR-05415-28 and 2-S07-RR-07083-23 sub 27, and travel support of the Deutsche Forschungsgemeinschaft to Dr. Beinbrech.

Received for publication 20 December 1990 and in final form 30 January 1992.

REFERENCES

Ashton, F. T. and F. A. Pepe. 1981. The myosin filament. VIII. Preservation of subfilament organization. *J. Microsc.* 123:93–104.

Ashton, F. T., G. Beinbrech, and F. A. Pepe. 1987. Subfilament organization in myosin filaments of the fast abdominal muscles of the lobster. *Homarus Americanus. Tissue Cell* 19:51–63.

Auber, J. 1967a. Particularites ultrastructurales des myofibrilles des muscles du vol chez des lepidopteres. *Compt. Rend. Ser. D.* 264:621–624.

Auber, J. 1967b. Remarques sur la structure des fibrilles des muscles du vol d'insectes, au niveau de la stri M. *Compt. Rend. Ser. D.* 264:2916–2918.

Aust, S., P. Hinkel, and G. Beinbrech. 1980. Evidence for four-stranded myosin filaments in honey bee flight muscle. *J. Muscle Res. Cell Motility.* 1:y448.

Baccetti, B. 1965. Perplexities and confirmations on the problem of the myosinic filament structure. *Boll. Soc. Ital. Biol. Sper.* 42:1181–1184.

Baccetti, B. 1966. New observations on the ultrastructure of the myofilament. *J. Ultrastruct. Res.* 13:245–256.

Beinbrech, G., F. T. Ashton, and F. A. Pepe. 1987. The invertebrate myosin filament: subfilament arrangement in the wall of tubular filaments of insect flight muscles. *J. Mol. Biol.* 201:557–565.

Beinbrech, G., U. Meller, and W. Sasse. 1985. Paramyosin content and thick filament structure in insect muscles. *Cell Tissue Res.* 241:607–614.

Bennett, P. M. and A. Elliot. 1981. The structure of the paramyosin core in molluscan thick filaments. *J. Musc. Res. Cell Motility.* 2:65–81.

Breuer, M., R. Achazi, and G. Beinbrech. 1982. The actin stimulated adenosine triphosphate activity g aggregates formed by myosin from insect flight muscle and paramyosin from ABRM. *J. Muscle Res. Cell Motility.* 3:503.

Bullard, B., B. Luke, and L. Winkelman. 1973. The paramyosin of insect flight muscle. *J. Mol. Biol.* 75:359–367.

Crowther, R. A., and L. A. Amos. 1971. Harmonic analysis of electron microscopic images with rotational symmetry. *J. Mol. Biol.* 60:123–130.

Crowther, R. A., R. Padron, and R. Craig. 1985. Arrangement of the heads of myosin in relaxed thick filaments from tarentula muscle. *J. Mol. Biol.* 184:429–439.

Epstein, H. F., G. C. Berliner, D. L. Casey, and I. Ortiz. 1988. Purified thick filaments from the Nematode Caenorhabditis elegans: evidence for multiple proteins associated with core. *J. Cell Biol.* 106:1985–1995.

Fan, S., M. Hong, and M. Chen. 1966. Electron microscope observations of the thick protein filaments of the myofibrils of the honey-bee flight muscle. *Kexue Tongbao.* 17:211–214.

Frank, J., M. Radermacher, T. Wagenknecht, and A. Verschoor. 1988. Studying ribosome structure by electron microscopy and computer-image processing. *Methods Enzymol.* 164:3–35.

Frank, J., B. Shimkin, and H. Douse. 1981a. SPIDER—A Modular Software System for Electron Image Processing. *Ultramicroscopy.* 6:343–358.

Frank, J., A. Verschoor, and M. Boublik. 1981b. Computer averaging of electron micrographs of 40S ribosomal subunits. *Science* (Wash. DC). 214:1353–1355.

Gilev, V. P. 1966a. Ultrastructure of thick filaments of muscle fibers. *Electron Microsc.* 2:689–690.

Gilev, V. P. 1966b. The ultrastructure of myofilaments. II. Further investigation of the thick filaments of crab muscles. *Biochim. Biophys. Acta.* 112:340–345.

Halvarson, M., and B. A. Alfzelius. 1969. Filament organization in the body muscles of the arrowworm. *J. Ultrastructure Res.* 26:289–295.

Hoyle, G. 1967. Diversity of stirated muscle. *Am. Zoologist.* 7:435–449.

Hoyle, G., and P. A. McNeill. 1968. Correlated physiological and ultrastructural studies on specialized muscles. *J. Exptl. Zool.* 167:487–521.

Ip, W., and J. Heuser. 1983. Direct visualization of the myosin cross bridge helices on relaxed rabbit psoas thick filaments. *J. Mol. Biol.* 171:105–109.

Kensler, R. W., and M. Stewart. 1983. Frog skeletal muscle thick filaments are three stranded. *J. Cell Biol.* 96:1979–1802.

Kensler, R. W., R. C. Levine, and M. Stewart. 1985. Electron microscopic and optical diffraction analysis of the structure of scorpion muscle thick filaments. *J. Cell Biol.* 101:395–401.

Levine, R. J. C., M. Elfvin, M. M. Dewey, and B. Walcott. 1976. Paramyosin in invertebrate muscle. 2. Content in relation to structure and function. *J. Cell Biol.* 71:273–279.

Maw, M. C., and A. J. Rowe. 1980. Fraying of A-filaments into three subfilaments. *Nature (Lond.)*. 286:412–414.

Nomomura, Y. 1974. Fine structure g the thick filaments in molluscan catch muscle. *J. Mol. Biol.* 88:445–455.

Pepe, F. A. 1982. The structure of vertebrate skeletal muscle myosin filaments. In Cell and Muscle Motility R. M. Dowben and J. W. Shay, editors. Plenum Press. New York. Vol. 2. 141–171.

Pepe, F. A., F. T. Ashton, C. Street, and J. Weisel. 1986. The myosin filament X. Observation of nine subfilaments in transverse sections. *Tissue Cell.* 18:499–508.

Pepe, F. A., F. T. Ashton, P. Dowben, and M. Stewart. 1981. The myosin filament. VII Changes in internal structure along the length of the filament. *J. Mol. Biol.* 145:421–440.

Pepe, F. A., and P. Dowben. 1977. The myosin filament. V. Intermediate voltage electron microscopy and optical diffraction studies of the substructures. *J. Mol. Biol.* 113:99–218.

Reedy, M. K. 1968. Ultrastructure of insect flight muscle I screw sense and structural grouping in the rigor cross-bridge lattice. *J. Mol. Biol.* 31:155–176.

Reger, J. F., and D. P. Cooper. 1967. A comparative study on the fine structure of the basalar muscle of the wing and the tibial extensor muscle of the leg of the lepidopteran. Archalarus lyciades. *J. Cell Biol.* 33:531–542.

Reger, J. F. 1967. A comparative study on striated muscle fibers g the first antenna and the claw muscle of the crab pinnixia sp. J. *Ultrastructure Res.* 20:72–82.

Stewart, M., R. W. Kensler, and R. C. Levine. 1985. Three-dimensional reconstruction of thick filaments from Limulus and scorpion muscle. *J. Cell Biol.* 101:402–411.

Stewart, M., F. T. Ashton, R. Lieberson, and F. A. Pepe. 1981. The myosin filament. IX. Determination of subfilament positions by computer processing of electron micrographs. *J. Mol. Biol.* 153:381–392.

Szent-Gyorgyi, A. G., C. Cohen, and J. Kendrick-Jones. 1971. Paramyosin and the filaments of molluscan "catch" muscles II native filaments: isolation and characterization. *J. Mol. Biol.* 56:239–258.

Van Heel, M. 1987. Similarity measure between images. *Ultramicroscopy.* 21:95–100.

Varrano-Marston, E., C. Franzini-Armstrong, and J. Haselgrove. 1984. The structure and disposition of cross bridges on deep-etched fish muscle. *J. Muscle Res. Cell Motility.* 5:363–383.

Winkelman, L. 1976. Comparative studies of paramyosins. *Comp. Biochem. Physiol. Pt. B* 55:391–397.

Wray, J. 1979. Structure of the backbone in myosin filaments of muscle. *Nature (Lond.)*. 227:37–40.